Angle-resolved photoemission from the NaCl (100) face

F.-J. Himpsel* and W. Steinmann
Sektion Physik der Universität München, München, Federal Republic of Germany
(Received 6 June 1977)

The angle and energy distribution of photoelectrons from the (100) face of NaCl single crystals were measured for photon energies ranging from 15 to 30 eV by use of synchrotron radiation. Critical points of the band structure along the line $\Gamma\Delta X$ of the Brillouin zone were derived from the data. The energies measured from the top of the valence band in eV are the following: $E(X'_4) = -2.4 \pm 0.2$, $E(X'_5) = -1.4 \pm 0.2$, $E(X_1) = 11.4 \pm 0.5$, $E(X_3) = 12.0 \pm 0.5$, $E(X'_4) = 17.0 \pm 0.5$, $E(\Gamma'_{25}) = 17.2 \pm 0.2$; and a minimum of the third conduction band on Δ_1 at 13.7 ± 0.5 eV. The assignment for $E(X_5)$ (21 eV) and $E(\Gamma_{12})$ (18.7 eV) is less certain. The evaluation is facilitated by the fact that many of the Bloch states on the $\Gamma\Delta X$ line do not contribute to the photoemission in the [100] direction since they do not contain the appropriate plane wave components.

I. INTRODUCTION

Angle-resolved photoemission results from metals and semiconductors have been explained fairly successfully by the volume band structure of these materials. For insulators, both the experimental situation and the status of the theory have not progressed as far. Photoemission from bulk insulators leads to charging which has to be compensated. Calculations suffer from the fact that the bands are far from being free-electron-like and that correlation effects (like the polarization of the surrounding of an electron or hole) have to be included. Therefore, calculations by various methods diverge not only in their energy scale but also in the sequence of certain conduction bands.

Angle-resolved experiments on insulators have started with alkali halides.[1] It has been shown that the angular distribution below the electron-electron scattering threshold is determined only by the conduction bands because of multiple electron-phonon scattering. Above threshold, the direct transition model starts to become valid as in the case of metals and semiconductors. Thus the problem of finding the correct conduction bands can be separated from the determination of the valence bands. Another advantage of insulators is the large escape depth of the photoelectrons in the order of several hundred angstroms below the threshold for electron-electron scattering. This guarantees that surface effects play a minor role, and the experimental results can essentially be accounted for by the volume band structure. In this paper we present angle-resolved photoemission data from NaCl (100) faces which cover a wide range of angles and energies. These experimental results contain information on the band structure in the whole Brillouin zone. We evaluate only the part of it pertinent to the $\Gamma\Delta X$ line which is most easily accessible and straightforward in the assignment.

II. EXPERIMENTAL

Experiments were performed at the DESY electron synchrotron with a 1-m normal incidence monochromator. The sample chamber is sketched in Fig. 1. It contains a fixed electron-energy analyzer of the filter-lens-type with a resolution of 0.2 eV and an acceptance cone of 3° full aperture. The escape angle of the photoelectrons with respect to the crystal axes is varied by turning the sample. The vacuum was in the 10^{-10}-Torr range. The samples could be cleaved *in situ* if the polar escape angle was fixed. In this case the samples were mounted on a rotary feedthrough, which could be attached in three different positions to the vacuum chamber such that the polar angle θ (measured from the normal of the sample surface) was 0°, 45°, and 72°, respectively. The results shown in Figs. 2 and 8 were taken in this experimental arrangement. If the polar angle had to be varied during the measurement, a manipulator with two rotations (full range for θ and 180° range for the azimuth ϕ) was applied. In this case, however, the samples could not be cleaved in the sample chamber. The surfaces prepared outside showed a reduced contrast of the angular distribution as compared to the samples cleaved

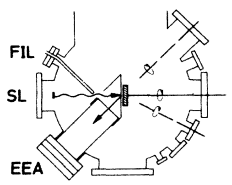

FIG. 1. Schematic drawing of the experimental arrangement. FIL is the hot filament for charging compensation, SL is the exit slit of the monochromator, EEA is the electron-energy analyzer. The electric-field vector lies in the plane of the figure.

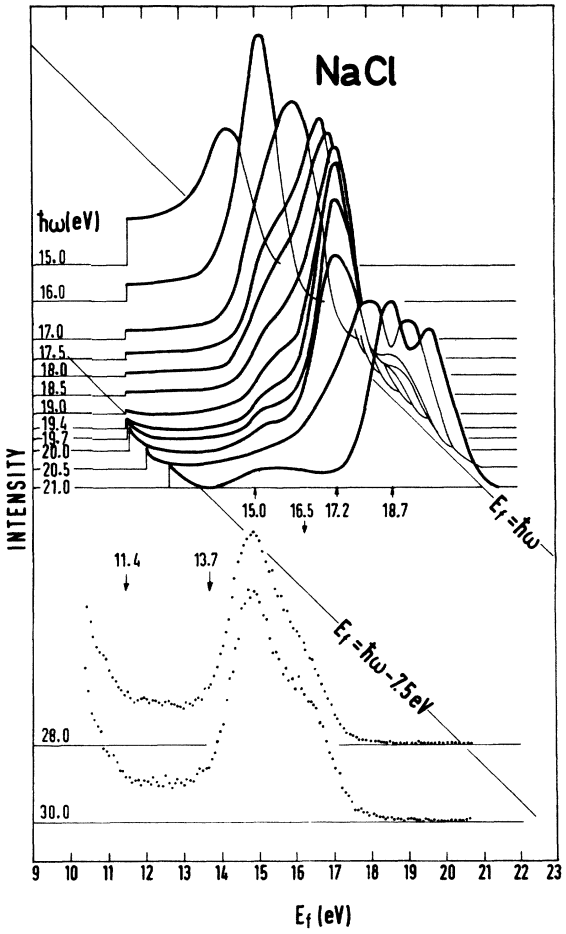

FIG. 2. EDC's of photoelectrons escaping normal to the (100) face of NaCl. The zero line is shifted proportional to the photon energy $\hbar\omega$. E_f is the energy measured from the top of the valence band. The EDC's are normalized to equal area except the EDC's for $\hbar\omega = 28$ and 30 eV where the intensity per incident photon is shown.

in situ but the structures remained. This is understandable in view of the results of Estel *et al.*[2] who found that H_2O desorbs almost completely from an air-cleaved NaCl (100) face below 10^{-8} Torr. Upon heating, a permanent hydroxide layer is formed. Therefore, we did not bake out the sample chamber with air-cleaved samples. The base pressure, in this case, was in the 10^{-9}-Torr range. The results shown in Figs. 6 and 7 were obtained in this configuration.

The charging of the samples was compensated by a cloud of low-energy electrons produced by a heated filament, which was outside the magnetic shielding of the drift space (see Ref. 1). The sample potential was stabilized to ± 0.3 eV by this method.

III. RESULTS AND DISCUSSION

A. General remarks

Three kinds of results have to be distinguished, depending on the scattering of the photoelectrons. They can be classified by the photon energy and the final energy of the electrons. The latter is divided into two ranges by the threshold energy for electron-electron scattering, which is the sum of the gap energy and the exciton energy.

Below threshold the escape depth is so large that several electron-phonon interactions take place before the photoelectron leaves the crystal. As a consequence, the photoelectron has lost any correlation to its initial position in the K space and thus the angular distribution does not depend on the initial state but only on the final state in this energy range. This has been verified in Ref. 1. The energy distribution of the photoelectrons at a given escape angle, however, is still influenced by the initial states because the energy loss due to phonons (about 25 meV for a single loss in NaCl) is small compared to the experimental energy resolution. We will refer to this process—direct excitation followed by several electron-phonon interactions—as quasidirect transitions.

Above the electron-electron scattering threshold the escape depth becomes smaller than the electron-phonon scattering length. This is the range of direct transitions as discussed usually for semiconductors and metals.

Finally, we will discuss a third type of experiment: Electrons excited to final energies high above the electron-electron scattering threshold can suffer subsequent energy losses and populate in this way the states below the electron-electron scattering threshold rather homogeneously. Both energy and angular distribution are determined solely by the final states in this case. These electrons are termed true secondaries.

B. Energy distributions for escape normal to the (100) face

1. Results

Energy-distribution curves (EDC's) for electrons escaping normal to the (100) surface are displayed in Fig. 2 for different photon energies $\hbar\omega$. The final energy of the electrons with respect to the top of the valence band E_f was determined from the high-energy edge of the EDC and the photon energy. The electron-electron scattering threshold is at $E_f = 16.5$ eV, as can be seen from the minimum energy loss of 7.5 eV in Fig. 2 and the energy gap value of 9.0 eV in Ref. 3. At threshold, the energy lost in the scattering process is used to create an exciton.

2. Selection rules

Among the final states in the conduction band only a restricted set is able to contribute to the emission in the direction of the surface normal. There are two selection rules:

(i) The reduced wave vector parallel to the surface $\vec{k}$ is a good quantum number if the crystal surface is periodic. For a Bloch state with reduced wave vector $\vec{K}$ which couples to the detected plane wave of wave vector $\vec{K}_v$ the conservation of $\vec{k}$ leads to the following relation:

$$\vec{K}^{\parallel} = \vec{K}_v^{\parallel} + \vec{g}. \tag{1}$$

$\parallel$ denotes the component parallel to the surface and $\vec{g}$ is a vector of the reciprocal surface lattice. The NaCl lattice is a fcc lattice with basis $(\frac{1}{2}a)$ 111 (a is the side length of the cube equal to 5.63 Å for NaCl). The reciprocal lattice of the (001) surface is simple cubic with the basis vectors (1, 1) and $(\bar{1}, 1)$ (in units of $2\pi/a$), if we assume that there is no superstructure (see the low-energy-electron-diffraction data in Ref. 4). The coupling-condition equation (1) is visualized in Fig. 3. For a given wave vector $\vec{K}_v$ in the vacuum the reduced $\vec{K}$ vectors of the Bloch states coupling to K_v are given by the intersection of at most two nonequivalent lines in the Brillouin zone with the energy surface. These lines can be constructed in the following way: Applying successively surface lattice vectors of the star $\langle 20 \rangle$ (in units of $2\pi/a$) to the rod $\vec{K}^{\parallel} = \vec{K}_v^{\parallel}$, one obtains a rod in the square $|K_x| \leq 2\pi/a$, $|K_y| \leq 2\pi/a$, which contains the projection of the first Brillouin zone (of the volume lattice) onto the surface. Starting with this rod one obtains a second one in the same $\vec{K}^{\parallel}$ area using a lattice vector of the star $\langle 11 \rangle$.

For emission in the [001] direction this construction yields $\vec{K}^{\parallel} = (0, 0)$ as the only possible wave vector in the surface Brillouin zone. All corresponding rods in three-dimensional $\vec{K}$ space are covered by the line $\Gamma\Delta X$ in the three-dimensional Brillouin zone.

(ii) In addition, the symmetry properties of a point in the surface Brillouin zone have an effect on the angular distribution. It has recently been shown by Hermanson[5] that only those final states can contribute to normal emission which are invariant under the point group operations about the surface normal. The point $\vec{K}^{\parallel} = (0, 0)$ has the full symmetry group of the reciprocal surface lattice 4 mm (C_{4v} in the Schoenfliess notation). Thus, the only representation that yields an outgoing wave of the type $\exp(iK_z z)$ is Δ_1 (A_1 in the Mulliken notation). [We neglect spin-orbit coupling which is about 0.1 eV for the valence band of NaCl (Ref. 3).] A Δ_2-type wave function $\psi(x,y,z)$ vanishes on the z axis because the sign of ψ changes if x and y are interchanged. [Taking $\psi(x,y,z) = -\psi(y,x,z)$ and setting $x = y = 0$ one obtains the relation $\psi(0,0,z) = -\psi(0,0,z)$, which results in $\psi(0,0,z) = 0$.] Hence a Δ_2-type Bloch function does not contribute to the photoemission normal to the (001) surface as it has no partial wave with vanishing component parallel to the surface. A similar proof is possible for the remaining representations Δ_2', Δ_1', Δ_5 because they are odd either with respect to x or y.

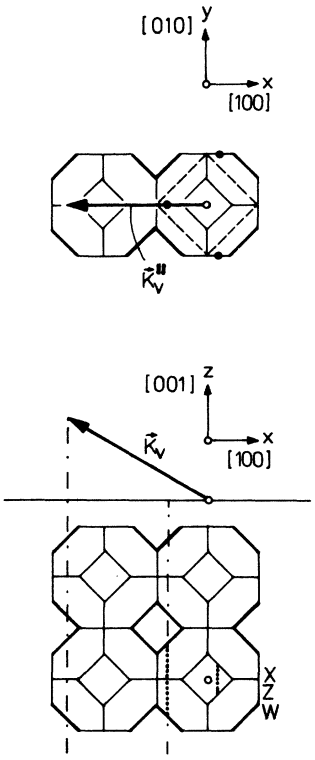

FIG. 3. Correlation between the wave vector of a plane wave in the vacuum $\vec{K}_v$, and the wave vectors of Bloch states that can contribute to the emission in the direction of $\vec{K}_v$ (dots). Shown are top and side view of the Brillouin zones for a fcc lattice and the two-dimensional Brillouin zone of the (001) surface (dashed). A detailed explanation is given in the text.

Finally, it should be mentioned that all transitions from either one of the two valence bands (Δ_1 and Δ_5 symmetry) are dipole allowed except $\Delta_1 \nrightarrow \Delta_2$ and $\Delta_1 \nrightarrow \Delta_2'$. The allowed initial-state symmetries are not restricted by additional selection rules for normal emission[5] since the light is polarized in the plane of incidence.

To summarize, only Δ_1-type final states can contribute to the photoemission in the direction of the surface normal for the (100) face of a fcc lattice.

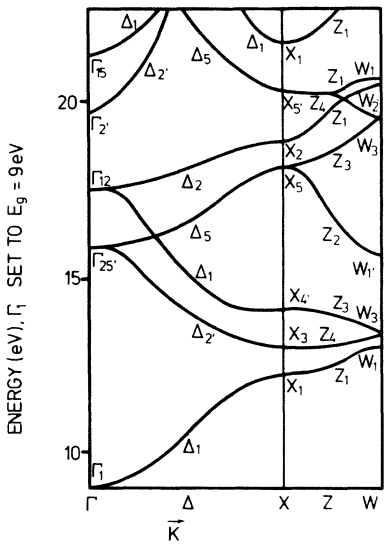

FIG. 4. Band structure of NaCl after Page and Hygh (Ref. 6).

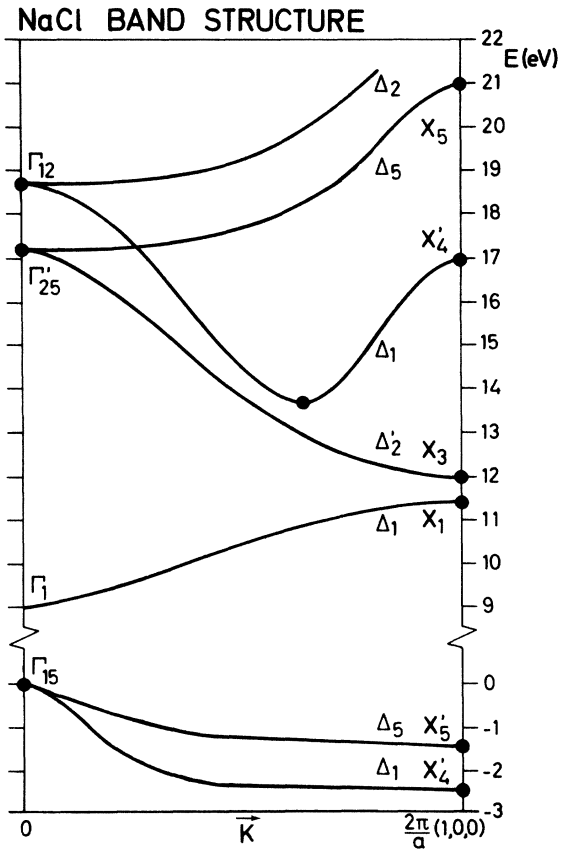

FIG. 5. Model band structure of NaCl obtained from the experimental results of this work (dots) in combination with recent calculations (Refs. 6 and 7). Energies are measured from the top of the valence band (Γ_{15}).

3. *Interpretation in terms of the band structure*

As a starting point we use the band structure calculated by Page and Hygh[6] shown in Fig. 4. The bands derived from our data are shown in Fig. 5. The EDC's with $\hbar\omega = 28$ and 31 eV (lower part of Fig. 2) originate from true secondaries. These electrons have lost the information about the initial energy and wave vector by the scattering. Hence, the EDC does not depend on the photon energy. The electrons are distributed rather uniformly over the conduction bands. Therefore, we expect that these EDC's reflect the density of states of the Δ_1 conduction bands. The intensity rise below $E_f = 11.4$ eV is attributed to electrons from the first conduction band which has symmetry Δ_1. The next band is of Δ_2' symmetry and does not contribute to the photoemission in [100] direction. This results in a region of low intensity which extends up to $E_f = 13.7$ eV. There the third band starts, which has again Δ_1 symmetry. Band-structure calculations indicate (see Table I) that the maximum of the first band is X_1 and the minimum of the third band on the Δ axis lies inside the Brillouin zone. The strongest contribution from the third band is observed around $E_f = 15$ eV which is about 1 eV higher than the minimum. A rise in the intensity above $E_f = 13.7$ eV can also be seen in the EDC of the quasidirect transition electrons (upper part of Fig. 2). Above the electron-electron scattering threshold there is a pinning of the peak of the EDC's to a final energy of 17.2 eV for photon energies between 18.5 and 20.0 eV. This indicates transitions from a valence band with strong dispersion (at least 1.5 eV) into a conduction band which is flat compared to this valence band. A similar but less pronounced structure is observed at $E_f = 18.7$ eV. We attribute the maximum at $E_f = 17.2$ eV to transitions from the lower valence band into final states around Γ_{25}' (e.g., $\Delta_1 \rightarrow \Delta_5$). The structure at 18.7 eV may correspond to a similar transition into final states around Γ_{12}. Two remarks should be made concerning this interpretation:

(a) The conduction bands Δ_5 and Δ_2 cannot contribute directly to the emission into the [001] direction for symmetry reasons. However, Δ_5 states near Γ_{25}' can be transformed into Δ_1 states by electron-phonon scattering without detectable change in energy. Electron-phonon scattering still occurs around $E_f = 17$ eV. This can be seen from the fact that the angular distribution does not depend on the initial state energy (see Ref. 1). Indeed, for the flat part of the Δ_5 band we expect a relatively small electron-phonon scattering length, because the group velocity is small. Typical electron-phonon scattering lengths[11] are well

TABLE I. NaCl band-structure data.

	Calculations (since 1969)					Experiment
Reference	8	6	7	9	10	3
Method[a]	EPM	APW	HF	HF	APW	Opt. refl.
$E_g = E(\Gamma_1) - E(\Gamma_{15})$	(9.0)[b]	(8.8)[b]	10.0	8.4	5.0	9.0
Initial states, measured from the top of the valence band (Γ_{15})						This work[c]
$E(X_5') - E(\Gamma_{15})$	−0.2	−0.2	−1.3	−0.6	−0.5	−1.4 ± 0.2
$E(X_4') - E(\Gamma_{15})$	−1.0	−0.6	−3.8	−1.5	−1.7	−2.4 ± 0.2
Final states, measured from the bottom of the conduction band (Γ_1)						
$E(\Gamma_n), E(X_n - \Gamma_1)$						
$E(X_1)$	1.0	3.1	2.9	3.4	3.4	2.4 ± 0.5
$E(X_3)$	1.0	4.0	3.0	2.0	2.6	3.0 ± 0.5
Minimum $E(\Delta_1)$	3.6	5.0	6.0		5.2	4.7 ± 0.5
$E(X_4')$	8.8	5.2	7.4	5.2	5.7	$8.0^{+0.5}_{-1.0}$
$E(X_5)$	7.3	9.0	11.3 (X_5')	10.3 (X_5')		12.0
$E(\Gamma_{25}')$	3.7	6.9	7.6	5.6	6.0	8.2 ± 0.2
$E(\Gamma_{12})$	4.2	8.4	10.0	8.1		9.7

All energies in eV.

[a] EPM—empirical pseudopotential method, APW—augmented plane wave, HF—Hartree-Fock.
[b] Values fitted to experimental data.
[c] The energies are measured from the top of the valence band. For the conduction bands $E_g = 9.0$ eV has been subtracted.

below the electron-electron scattering length of 80 Å derived from our data[12] for $E_f = 17.2$ eV. On the other hand, an electron that arrives in the Δ_1 bands has a much higher group velocity and may escape without further phonon scattering. For the Δ_2 band such an explanation is not possible, because the electron-electron scattering length is too small (about 8 Å at $E_f = 18.7$ eV). Only the Δ_1 band connected to the point Γ_{12} contributes to the photoemission in direction of the surface normal.

(b) The strong decrease of the emission intensity above the electron-electron scattering threshold modulates the shape of the EDC's. It could be argued that this modulation is responsible for the main peak remaining constant for $18.5 < E_f < 20.0$ eV. However, this would not be compatible with our observation that the EDC's behave differently in other escape directions.

For photon energies above 20 eV the EDC consists of two maxima which move to higher energies as the photon energy is increased such that $E_i = E_f - \hbar\omega$ remains constant. Therefore they are interpreted as maxima in the density of the initial states at the points X_5' and X_4'. In this range of final energies, all states of Δ_1 symmetry must be evanescent according to the calculation in Ref. 6. Indeed, we observe such a low photoemission intensity that the corresponding escape depth is less than 4 Å. We obtain −2.4 eV for the initial energy of X_4' and −1.4 eV for X_5'.

C. Angular distribution of the intensity

Figure 6 shows energy distributions of true secondaries for various escape directions in the two symmetry planes (010) and $(\bar{1}10)$. Like the curves shown in the lower part of Fig. 2 ($\hbar\omega = 28$ and 30 eV) these EDC's are insensitive to the photon energy and can be interpreted using only the conduction bands. The inset compares an angle-integrated EDC from an evaporated film[13] with the angle-resolved data. The two peaks *C* and *D* appear for different escape directions, *C* at high polar angles in the (010) plane, *D* for escape normal to the (001) surface. *F* coincides with the onset of electron-electron scattering. Peak *D* is the same as the one shown in the lower part of Fig. 2 and corresponds to the minimum of the third conduction band on the Δ axis. To account for maximum *C* one has first to determine which part of the Brillouin zone can contribute to the emission in this range of energy and escape angle. The component of $\vec{K}_v$ parallel to the surface (see Fig. 3) can be calculated from the measured energy and escape direction by the relation

$$|\vec{K}_v^{\parallel}| = [(2m/\hbar^2)(E - E_v)]^{1/2} \sin\theta\,, \tag{2a}$$

which for NaCl takes the form

$$|\vec{K}_v^{\parallel}|/(2\pi/a) = 0.459[(E - E_v)/\mathrm{eV}]^{1/2} \sin\theta\,. \tag{2b}$$

E_v is the vacuum level and θ is the angle between the escape direction and the surface normal.

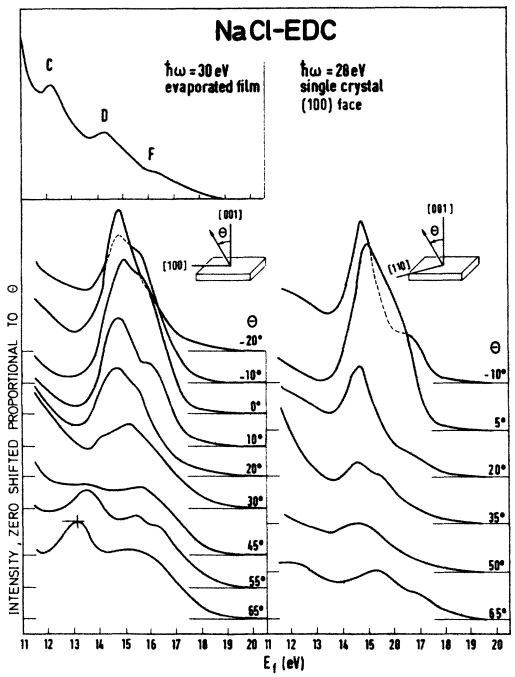

FIG. 6. EDC's of secondaries produced by electron-electron scattering for different escape directions. The insert is taken from Ref. 13. Compared to Ref. 13, our EDC's are shifted by 0.5 eV to higher energy because we use a different method to determine the upper edge of the EDC's.

With $E_f = 13$ eV, $E_v = 9$ eV (Ref. 14) and $\theta = 65°$, Eq. 2(b) yields $|\vec{K}_v^{\parallel}|/(2\pi/a) = 0.83$. The possible $\vec{K}$ values of the contributing Bloch states are shown as dotted lines in Fig. 3. The method to construct these lines has been described in Sec. III B 2.

The band structure in Fig. 4 shows a minimum in this E, $\vec{K}$ range at X_3, which is the lowest point of the second band. States on the dotted line inside the Brillouin zone compatible with X_3 [$\bar{1}$00] have odd symmetry with respect to the plane of observation (010). Hence, they cannot contribute to the emission in this mirror plane.[5] However, there is an equivalent point in the surface lattice (see upper part of Fig. 3) which corresponds to the dotted line on the boundary of the volume Brillouin zone, shown in the lower part of Fig. 3. States on this line compatible with X_3 [010] have even symmetry with respect to the plane of observation. Therefore, these states on the surface of the Brillouin zone will give rise to peak C in Fig. 6. Hence, by studying the EDC at oblique escape angles we have found a piece of the band structure on the Δ axis which was missing in the emission normal to the (100) face.

For a quasidirect transition, the angular distribution of the photoemission intensity at fixed final energy ($E_f = 15.7$ eV) is represented in Fig. 7 by lines of equal intensity. The azimuth ϕ is related to the component of the $\vec{K}_v$ vector parallel to the surface, $\vec{K}_v^{\parallel}$; ⟨10⟩ means that $\vec{K}_v^{\parallel}$ has a direction equivalent to the [10] direction. This corresponds to the {100} escape planes. There is low intensity in the azimuthal ⟨11⟩ directions, corresponding to the {110} escape planes. Bright spots are at $\theta = 55°$, ϕ corresponding to the ⟨10⟩ directions—called peak A—and at $\theta = 65°$, $\phi = \pm 10°$ with respect to the ⟨11⟩ directions—called peak B. Equation (2b) yields for A, $K_v^{\parallel}/(2\pi/a) = 0.97$.

In this case the construction described in Sec. III B 2 (Fig. 3) shows that the four corners of the surface Brillouin zone ([10], [01], [$\bar{1}$0], and [0$\bar{1}$]) contribute. These points correspond to four rods in the reciprocal volume lattice which comprise the lines $WZXZW$ along the z direction of the volume Brillouin zone. The symmetry of the Bloch states on the Z line is 2 mm(C_{2v}). The states of the four rods have to be combined to form the total wave function which has the symmetry 4 mm of the reduced wave vector parallel to the surface. If the total wave function is an odd function of y, it will vanish on the xz plane, which is the plane of observation. Therefore, no contribution is expected from such states. The symmetry of the total wave function depends on the symmetry of the Z-type Bloch functions of the four rods which have to be combined. Three cases can be distinguished.

(a) For Z_1 symmetry, the Bloch function is even with respect to both x and y. In this case, the total wave function will also be an even function of y. Hence, Z_1 states will contribute to the observed photoemission.

(b) For Z_3 and Z_4 symmetry, the Bloch functions are even with respect to x and odd with respect to y or vice versa. A Bloch function which

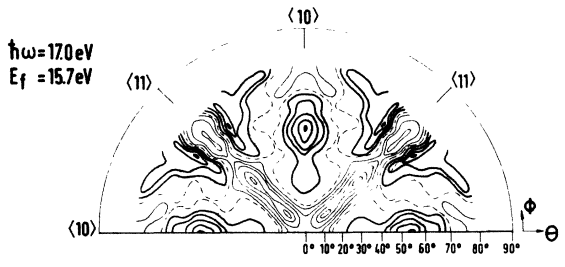

FIG. 7. Angular distribution of the photoelectron intensity from a NaCl (001) face for a photon energy $\hbar\omega = 17$ eV and electron energy $E_f = 15.7$ eV (measured from the top of the valence band). The polar angle θ and the azimuth ϕ are represented in stereographic projection. ⟨10⟩ and ⟨11⟩ mark a ϕ corresponding to the {100} and {110} escape planes, respectively. Heavy lines denote intensity maxima, thin lines minima.

is an even function of x and an odd function of y in the rod $\vec{K}''=[10]$, is odd with respect to x and even with respect to y in the rod $\vec{K}''=[01]$. Hence, a linear combination of the four rods leads to a total wave function which is not necessarily odd with respect to y. Consequently, Z_3 and Z_4 states can contribute to the observed photoemission in general.

(c) For Z_2 symmetry, the Bloch functions are odd functions of both x and y. A linear combination of the four rods will also lead to an odd function of y. Z_2 states will therefore not contribute to the photoemission in the xz plane.

For the overall behavior of the band structure we use again the calculation of Page and Hygh[6] shown in Fig. 4. The final energy $E_f = 15.7$ eV is in the range of the fourth conduction band which has Z_2 symmetry. Because of symmetry arguments given above, this band cannot contribute to the photoemission in the direction in which peak A is observed. Consequently, peak A must originate from the third or fifth conduction band which have symmetry Z_3. The top of the third band is point X_4', the bottom of the fifth band is X_5. Thus, we expect peak A to disappear in a certain energy range corresponding to the energy gap between the third and fifth band on the Z axis. The dependence of the intensity of peak A on the final energy will show whether $E_f = 15.7$ eV lies in the third or fifth conduction band. Figure 8 shows

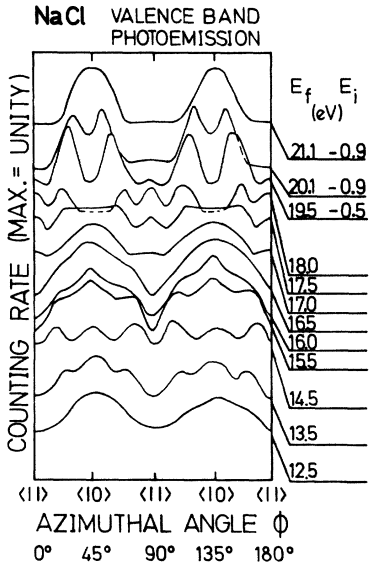

FIG. 8. Azimuthal pattern of the valence band photoemission from the NaCl (001) face. The zero line is shifted proportional to the final state energy E_f as indicated on the right-hand side of the figure. $E_i = E_f - \hbar\omega$. The curves are normalized with respect to their maximum value (from Ref. 1).

an azimuthal intensity distribution with E_f as the parameter. In the range of quasidirect transitions the initial energy E_i does not have to be specified since the angular distribution is independent of E_i.[1] In the direct transition regime, i.e., for E_f above the threshold for electron-electron scattering, E_i is also given. The data were taken at a polar angle θ of 45° which, according to Eq. (2b), corresponds approximately to the boundary of the Brillouin zone $|\vec{K}''| = 2\pi/a$ in the energy range in question. The maximum in the ⟨10⟩ direction in Fig. 8 corresponds to peak A in Fig. 7. This maximum occurs at all final energies except in the range $17 < E_f < 21$ eV. The boundaries of this energy gap correspond to the points X_4' and X_5 in the band structure. In some calculations this point has symmetry X_5'. In this case, transitions from the valence bands are forbidden in contrast to the rather strong transition which we observe.

All obtained energy values of critical points are collected in Table I and compared to more recent band-structure calculations. To eliminate the rather high uncertainity of the calculations concerning the band-gap energy, we have related our results for the conduction bands to the bottom of the conduction band using the experimental band-gap value given in Ref. 3.

IV. CONCLUSION

We have shown in this paper that angle-resolved photoemission data can be used to determine critical points of three-dimensional valence and conduction bands. This is achieved without detailed calculation using only qualitative prior knowledge of the bands in symmetry directions and taking into account the angular characteristic of the wave function. The key information is given by the dependence of the observed structures on photon energy. This shows the advantage of synchrotron radiation as a light source for such experiments. Comparing our results with band-structure calculations, it appears that Hartree-Fock calculations including polarization corrections give the best values for the energies of the critical points. An empirical pseudopotential calculation[8] agrees poorly with our data. It should be possible, however, to obtain improved pseudopotential parameters from our results. With such a pseudopotential it is rather straightforward to calculate the angular distribution of the photoemission for all escape angles (see Refs. 12 and 15). The result could be compared with the experimental data shown in Fig. 7. This would be a test if the pseudopotential yields the correct conduction bands in the whole Brillouin zone. The improved band structure may be used to calculate

optical absorption spectra. Comparison with experimental results could show whether or not excitations into high conduction-band states are influenced by excitonic effects.

ACKNOWLEDGMENT

This work was supported by Deutsches Elektronensynchrotron DESY, Hamburg.

---

*Present address: IBM Thomas J. Watson Research Center, Yorktown Heights, N.Y. 10598.

[1]F. J. Himpsel and W. Steinmann, Phys. Rev. Lett. 35, 1025 (1975).

[2]J. Estel, H. Hoinkes, H. Kaarmann, N. Nahr, and H. Wilsch, Surf. Sci. 54, 393 (1976).

[3]D. M. Roessler and W. C. Walker, Phys. Rev. 166, 599 (1968).

[4]J. Bandet, L. Touzillier, A. Malavaud, and Y. Quemener, Surf. Sci. 51, 174 (1975).

[5]J. Hermanson, Solid State Commun. 22, 9 (1977).

[6]J. L. Page and E. H. Hygh, Phys. Rev. B 1, 3472 (1970).

[7]N. O. Lipari and A. B. Kunz, Phys. Rev. B 3, 491 (1971).

[8]C. Y. Fong and M. L. Cohen, Phys. Rev. 185, 1168 (1969).

[9]F. Perrot, Phys. Status Solidi B 52, 163 (1972).

[10]J. S. Melvin and T. Smith, Phys. Status Solidi B 49, 173 (1972).

[11]J. Llacer and E. L. Garwin, J. Appl. Phys. 40, 2766 (1969).

[12]F. J. Himpsel, thesis (University of München, 1976) (unpublished).

[13]G. J. Lapeyre, J. Anderson, J. A. Knapp, and P. L. Gobby, in *Vacuum Ultraviolet Radiation Physics*, edited by E. E. Koch, R. Haensel, and C. Kunz (Vieweg/Pergamon, Braunschweig, 1974), p. 380.

[14]W. Pong and J. A. Smith, Phys. Rev. B 9, 2674 (1974).

[15]F. J. Himpsel and W. Steinmann, in Proceedings of an International Symposium Noordwijk, Netherlands, ESA SP 118 REV. 1, Nov. 1976 (unpublished), p. 137.